International Journal of Materials Science and Technology Studies
ISSN: 3006-7693 (Print), ISSN: 3006-3744 (Online) | Volume 5, Number 2, Year 2026
DOI: https://doi.org/10.62051/ijmsts.v5n2.10
Journal homepage: https://wepub.org/index.php/IJMSTS/index

Study on Laser Welding of Advanced High Strength Martensite Steel

Yang Shen

University of Shanghai for Science and Technology, Shanghai, China
shenyang32100@163.com

ABSTRACT

The growing demand for lightweight yet crashworthy automotive structures has promoted the use of 1.5 GPa grade martensitic steels (MS1500 1). However, laser welding of such ultra high strength materials is challenged by heterogeneous microstructures and severe hydrogen induced delayed cracking (HIDC) risks. This study systematically investigates the laser welding behavior and hydrogen embrittlement susceptibility of MS1500 1, focusing on three aspects: (1) the effect of surface oil contamination (oil free, 1.5 g/m² as received, and 3.0 g/m² excessive lubricant) on microstructural evolution and mechanical performance of laser lap welded (L bend) and butt welded joints; (2) the hydrogen permeation and diffusion behavior in the base metal using electrochemical permeation tests; and (3) the correlation between microstructural features of distinct heat affected subzones, local hardness distribution, and overall joint integrity. Comprehensive microstructural characterization (optical microscopy, scanning electron microscopy, X ray diffraction), mechanical evaluation, and hydrogen permeation measurements reveal that surface oil significantly alters the weld thermal cycle and hydrogen uptake, leading to pronounced softening and increased HIDC susceptibility. The results establish a fundamental understanding of hydrogen trapping characteristics and mechanical reliability of laser welded MS1500 1 joints, providing a scientific basis for mitigating delayed cracking and developing robust welding protocols for ultra high strength steel components in automotive manufacturing.

KEYWORDS

Martensite steel; Hydrogen embrittlement sensitivity; Laser welding

1. INTRODUCTION

The increasing demand for vehicle lightweighting and enhanced crashworthiness in the automotive industry has driven the extensive adoption of Advanced High-Strength Steels (AHSS), particularly those with tensile strengths reaching 1.5 GPa and above. Among these, martensitic steels (MS) and dual-phase (DP) steels are favored for structural components due to their exceptional strength-to-weight ratio. However, the deployment of these ultra-high-strength materials necessitates reliable joining techniques, with laser welding being a preferred method for producing tailored blanks and structural assemblies.

While laser welding offers advantages in terms of speed and precision, the rapid thermal cycles inherent to the process create heterogeneous microstructures across the weld joint. As reported by Wang et al. [1] in their investigation of laser-arc hybrid welded high-strength steel joints, the weld zone and heat-affected zone (HAZ) are predominantly composed of lath martensite, with the fusion zone exhibiting a hardness of 470–500 HV, the HAZ reaching 480–530 HV, and a distinct softened zone exhibiting hardness below 350 HV. This microstructural gradient, combined with the material's

inherently high sensitivity to hydrogen embrittlement (HE), renders 1.5 GPa steel joints highly susceptible to hydrogen-induced delayed cracking (HIDC). As noted by Li et al. [2], the heat input during laser welding significantly influences the width and severity of the softened zone, which in turn governs the fracture location and overall joint integrity in ultra-high-strength dual-phase steels.

The risk of HIDC is further exacerbated by practical manufacturing conditions [3]. The presence of anti-corrosion oils and additional stamping lubricants on the steel surface introduces external hydrogen sources during welding. Furthermore, automotive structural parts often undergo plastic deformation prior to assembly, introducing pre-strain which can significantly alter the hydrogen trapping behavior and diffusion kinetics within the complex-phase microstructure. A patent by an industry research group highlights that cold cracking in high-strength steel laser welds occurs under the combined action of restraint stress, hardened microstructure, and diffusible hydrogen, with the cracking exhibiting a characteristic incubation period ranging from hours to months. [4-6] This delayed nature poses significant safety risks in automotive applications. Additionally, research on high-strength martensitic steel (H750MS and TZ750MS) has demonstrated that hydrogen-induced delayed cracking constitutes the primary failure mechanism in these materials, with the density and distribution of hydrogen traps—such as (Ti, Nb)C and Fe_3C precipitates—playing a decisive role in determining the delayed cracking susceptibility [7]. Therefore, a comprehensive understanding of the coupling effects between laser welding parameters, surface contamination, pre-strain, and microstructural evolution on hydrogen-induced failure is critical for the safe application of these materials.

This study systematically investigates the laser welding behavior and hydrogen embrittlement susceptibility of a 1.5 GPa grade martensitic steel (designated MS1500-1). The research encompasses three primary objectives: (1) to elucidate the influence of varying surface oil conditions (oil-free, as-received 1.5 g/m², and excessive 3.0 g/m² lubricant) on the microstructural evolution and mechanical properties of laser lap-welded (L-bend) and butt-welded joints; (2) to characterize the hydrogen permeation and diffusion behavior in the base metal (BM) through electrochemical permeation testing; and (3) to correlate the microstructural features of distinct heat-affected subzones with the local hardness distribution and the overall joint integrity. By integrating microstructural analysis via Optical Microscopy (OM), Scanning Electron Microscopy (SEM), and X-ray Diffraction (XRD) with mechanical evaluations and hydrogen permeation measurements, this work aims to establish a fundamental understanding of the hydrogen trapping characteristics and mechanical reliability of laser-welded MS1500-1 steel joints. The findings are expected to provide a scientific basis for mitigating delayed cracking in automotive manufacturing and to inform the development of robust welding protocols for ultra-high-strength steel components.

2. METHODS

The chemical composition of the cold-rolled martensitic steel used in the study is shown in Table 1.

Table 1. Chemical compositions of the investigated martensite steel specimens

	C	Si	Mn	P	S	B	Al	N	Nb	Ti
MS-1	0.19	0.2	1.62	0.006	0.0006	0.0003	0.03	0.004	0.011	0.024
MS-2	0.23	0.19	1.08	0.008	0.0006	0.0025	0.03	0.004	0.027	0.019

2.1. Microstructure Observation

The metallographic specimen measures 10.0 mm x 10.0 mm x 1.1 mm in size. It is sequentially polished using 400#, 800#, 1200#, 1500#, and 2000# sandpaper, and then polished to achieve a mirror-like finish without any scratches. An alcohol solution containing 4.0% nitric acid (by volume) is used for etching, with an etching duration of 10-12 seconds. The microstructure of the material is

analyzed and characterized using a DMI8A inverted optical microscope (OM) and a FEI QUANTA450 scanning electron microscope (SEM).

2.2. Electrochemical Hydrogen Charging

Utilizing a wire cutting machine, MS-1 and MS-2 steel plates with different compositions were processed into tensile specimens along the rolling direction. The dimensions of the gauge length section of the tensile specimens were 25.0 mm x 5.0 mm x 1.1 mm. The gauge length section was sequentially polished using 400#, 800#, 1000#, 1200#, and 1500# sandpaper. To prevent the parts outside the gauge length section from participating in electrochemical hydrogen charging, insulating waterproof tape was used to seal them. The electrochemical hydrogen charging experiment employed an aqueous solution of 0.1 mol/L H2SO4 + 1 g/L CH4N2S as the electrochemical hydrogen charging solution, with high-purity platinum wire as the anode, and the reserved gauge length section of the hydrogen-charged specimen as the cathode.

2.3. Mechanical Property Testing

The tensile test samples were subjected to conventional tensile testing using a UTM4304 material tensile testing machine (Shenzhen Sansi Zongheng Technology Co., Ltd.). The tensile rate was set at 0.5 mm/min, and the strain was recorded using an extensometer to calculate the tensile strength and elongation of MS steel samples with different compositions.

The residual hydrogen-charged solution on the surface of the pre-charged hydrogen sample was rinsed and dried. Slow strain rate tension (SSRT) tests were conducted at a tensile rate of 0.015 mm/min, and the tensile strength and elongation of the sample under different hydrogen-charging conditions were calculated.

3. RESULTS

3.1. Microstructure Characterization

Using X-ray diffraction analysis (XRD), the phase analysis of the base material MS1500-1 advanced high-strength martensitic steel was conducted. The phase composition is shown in Figure 1. The results indicate that MS1500-1 advanced high-strength martensitic steel consists of two phases: ferrite and martensite, exhibiting a BCC structure.

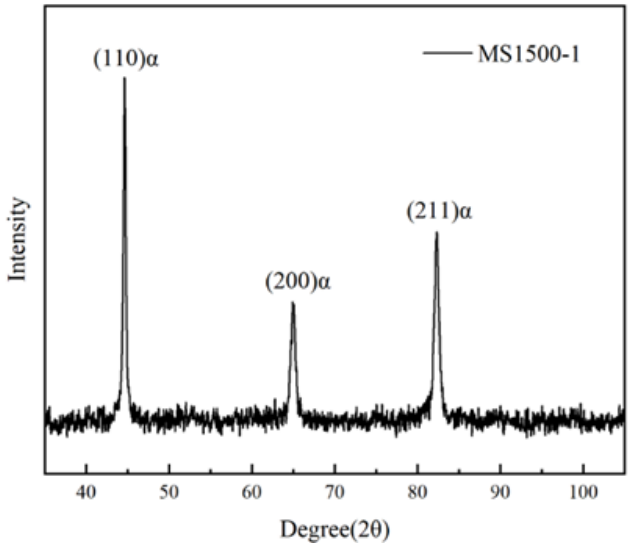

Figure 1. XRD pattern of MS1500-1

Using X-ray diffraction analysis (XRD), the phase analysis of the base material MS1500-1 advanced high-strength martensitic steel was conducted. The phase composition is shown in Figure 1. The results indicate that MS1500-1 advanced high-strength martensitic steel consists of two phases: ferrite and martensite, exhibiting a BCC structure.

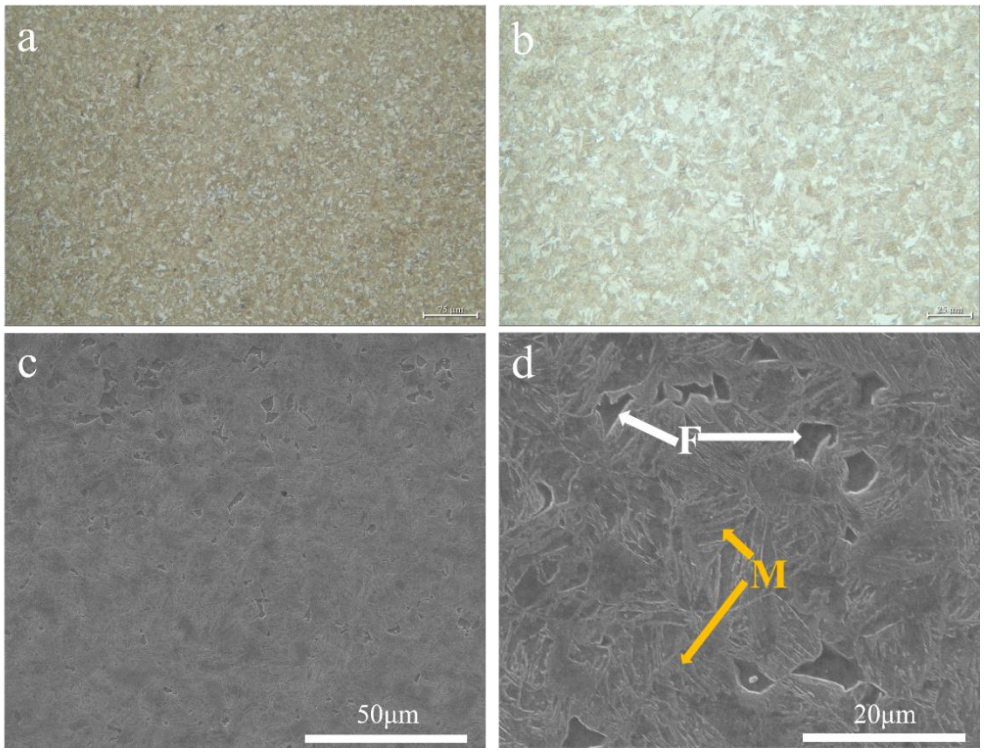

Figure 2. Microstructure analysis of MS1500-1 base material. (a, b) OM images; (c, d) SEM images. Where F represents ferrite structure and M represents martensite structure

3.2. Laser Welding

3.2.1. Laser Welding Process And Parameters

The TruLaser Cell 7020 laser equipment was utilized to perform splice welding on 1500MS-1 steel under two distinct welding process parameters. Refer to Figure 3 for the schematic diagram of the splice welding. The laser welding device primarily consists of a device platform, fixtures, and laser components. The MS1500-1 steel plates for splicing measure 200 mm in length, 100 mm in width, and 1.1 mm in thickness. The rolling direction is perpendicular to the welding direction, and the splicing method employed is butt welding.

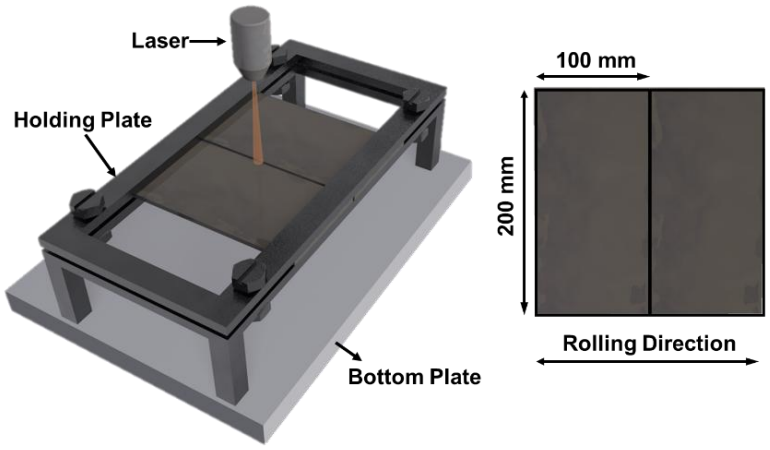

Figure 3. Splicing and welding schematic diagram

Two sets of process parameters were adopted for laser butt welding, with main controlled variables including laser power, welding speed, defocus distance and shielding gas (argon). The parameters are listed in Table 2.

Table 2. Laser welding process parameters for splicing

Parameter / Number	Laser power/kW	Speed/m·min^{-1}	Defocus/mm	Shielding gas/L·min^{-1}	Heat input/J•mm^{-1}
1(20cm*10cm)	2	5	-2	20	24
2(20cm*10cm)	2	5	-3	20	24
1(2cm*10cm)	2	9	-2	15	13.33
2	5	9	-2	15	33.33
3	1	9	-2	15	6.67
4	1	4.5	-2	15	13.33
5	1	3	-2	15	20
6	1	1.8	-2	15	33.33
7	2	7.2	-2	15	13.67
8	2	6	-2	15	20
9	2	10.2	-2	15	11.76
10	3	10.2	-2	15	17.65
11	1	4.2	-2	0	14.29
12	1	3.6	-2	0	16.67

3.2.2. Mechanical Properties of Butt Welded Joints

Tensile tests were conducted to characterize the strength of butt welded samples. The specimen dimensions are shown in the figure. Tensile tests were performed on a UTS4304 universal testing machine, with elongation recorded by an extensometer at a strain rate of 0.5 mm/min. The stress-strain behavior during tension was observed to analyze the tensile mechanical properties of welded samples. The properties of samples welded with different processes are shown in Figure 4. Figure 4 shows the tensile mechanical properties of MS1500-1 base metal, with a tensile strength of 1547.13 MPa and elongation of 10.64%. The sample welded with parameters of 2 kW laser power, 5 m/min welding speed, -2 mm defocus distance and 20 L/min shielding gas flow has a tensile strength of 1087.5 MPa (70.3% of the base metal) and elongation of 2.99%. The sample welded with 2 kW laser power, 5 m/min welding speed, -3 mm defocus distance and 20 L/min shielding gas flow shows consistent tensile mechanical properties in repeated tests, with a tensile strength of 1131.73 MPa (73.1% of the base metal) and elongation of 2.45%. Changing the defocus distance from -2 mm to -3 mm increases tensile strength but decreases elongation. Adjusting process parameters can achieve the goal of making the welded sample strength close to that of MS1500-1 base metal while ensuring certain elongation. Table 3 summarizes the tensile strength and elongation of welded samples under different process parameters.

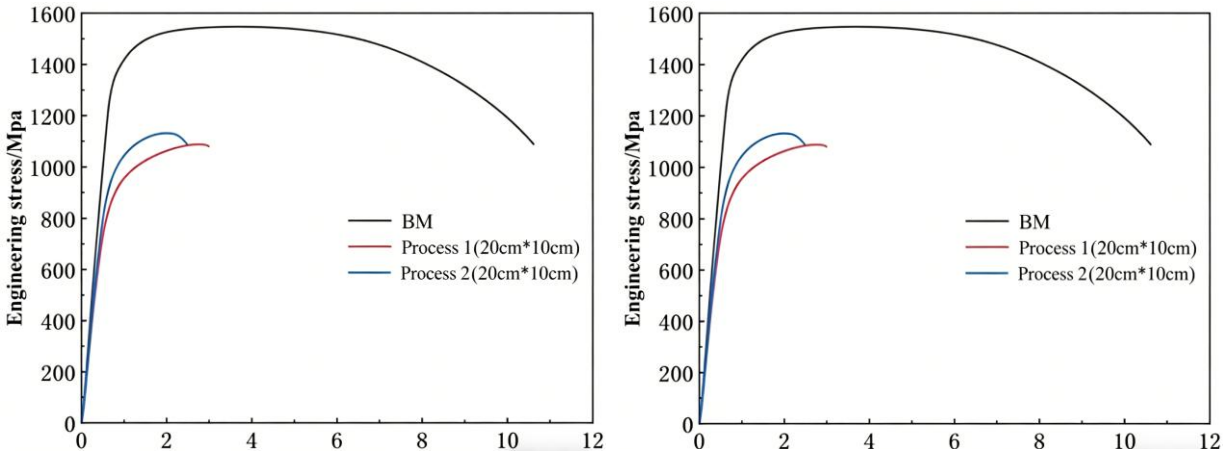

Figure 4. Stress-strain curve of MS-1 base material and welded joint

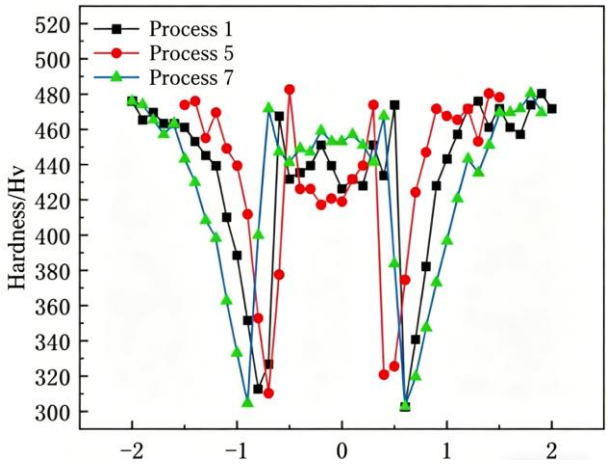

Figure 5. Microhardness of MS-1 welded joints with different processes

Microhardness testing was used to characterize the mechanical properties of butt welded joints. Vickers hardness tests were carried out on welded samples using an HVS-1000Z digital microhardness tester with a test load of 500 g and holding time of 15 s. The test area covers the entire cross-section of the welded joint, including base metal zone, heat-affected zone (HAZ), critical HAZ, fine-grained zone, coarse-grained zone and weld zone, to systematically analyze the hardness distribution characteristics of different zones during welding and the effects of different process parameters on the mechanical properties of butt welded joints, as shown in Figure 5. The hardness first increases, then decreases and finally increases with the distance from the weld center, which can be divided into three zones: hardened zone, softened zone and base metal zone. The hardened zone consists of weld zone, coarse-grained zone and fine-grained zone. The hardened zone has high microhardness due to the fast cooling rate after welding, with most microstructures being martensite, usually the hardest zone of the joint. There are hardness peaks on both sides of the hardened zone, located in the fine-grained zone. The fine-grained zone has a lower welding temperature and the fastest cooling rate, with finer martensite laths, leading to the highest hardness due to grain refinement strengthening. The softened zone includes critical HAZ and HAZ, where martensite tempering softening causes hardness reduction.

When the laser welding process is fixed at 2 kW power, -2 mm defocus distance and 15 L/min argon flow, reducing the welding speed from 9 m/min to 7.2 m/min (increasing heat input from 13.33 J/mm to 16.67 J/mm), the softening degree of the softened zone relative to the base metal shows little difference, with a hardness drop of about 160 Hv and softened zone width of 1.6 mm; the peak

hardness of the fine-grained zone is about 470 Hv; the weld center hardness is about 440 Hv; the width of the critical HAZ increases by 1 mm for Process 7 compared with Process 1.

When the process is fixed at -2 mm defocus distance and 15 L/min argon flow, reducing the power from 2 kW to 1 kW and welding speed to 3 m/min (increasing heat input to 20 J/mm), the softening degree of the softened zone still shows little difference, with the softened zone width reduced to 1.4 mm; the peak hardness of the fine-grained zone increases to 482 Hv, while the weld center hardness decreases to about 420 Hv.

3.2.3. Microstructure of Butt Welded Joints

Welded samples with good surface quality were obtained by adjusting process parameters, and the joint microstructure was characterized by optical microscopy, as shown in Figure 6. Figures 6(a–c) are OM images of laser welded joints under different welding processes, and (d–f) are their magnified views. The weld width and microstructure comparison of different zones of welded joints under different processes were obtained through analysis.

When the process is fixed at 2 kW power, -2 mm defocus distance and 15 L/min argon flow, reducing the welding speed from 9 m/min to 7.2 m/min (heat input from 13.33 J/mm to 16.67 J/mm), the weld width increases from about 1270 μm to 1380 μm. When the power is reduced from 2 kW to 1 kW and welding speed to 3 m/min (heat input to 20 J/mm), the weld width decreases to about 1040 μm.

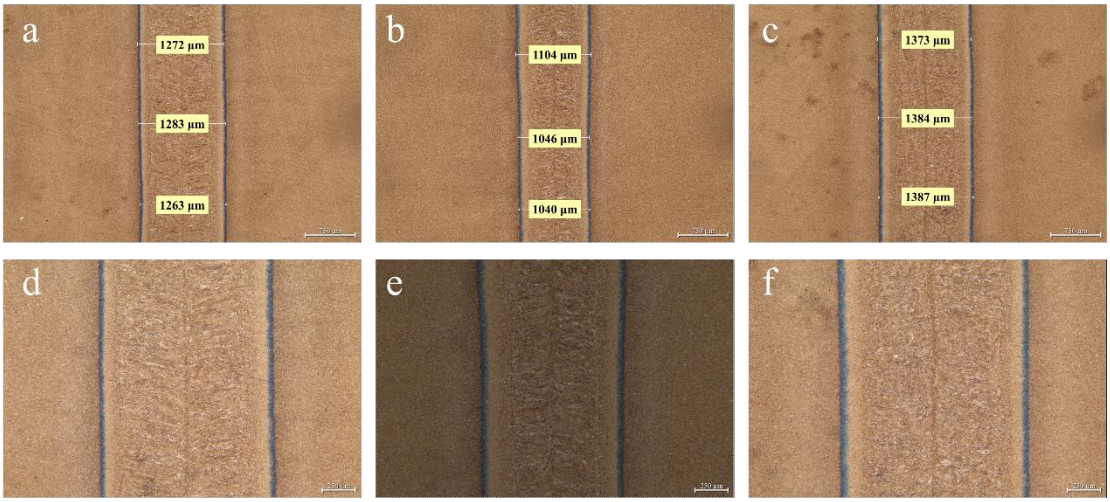

Figure 6. Metallographic images of 2cm×10cm welded joints under different processes. (a, d) Process 1; (b, e) Process 5; (c, f) Process 7

3.3. Hydrogen Permeation Behavior

An electrochemical workstation was used to evaluate hydrogen permeation by measuring the current generated during hydrogen diffusion and aggregation in the metal based on hydrogen diffusion and trapping behavior. Hydrogen was introduced electrochemically; hydrogen atoms diffuse into the metal lattice and form clusters or hydrides over time, generating electron flow and hydrogen permeation current to assess hydrogen permeability and hydrogen trap density in MS1500-1.

Hydrogen permeation tests were conducted on MS1500-1 base metal, and the hydrogen permeation curve is shown in Figure 7. The steady-state current density (I), sample thickness (L) and relaxation time (tL) of two tests were calculated and statistically analyzed. Hydrogen permeability (J∞L), effective hydrogen diffusion coefficient (Deff), apparent hydrogen concentration (Capp) and hydrogen trap density (NT) were obtained via Formulas (1)–(4), as listed in Table 3.

$$J_{\infty}L = \frac{I_{\infty} \times L}{F \times A} \quad (1)$$

$$D_{eff} = \frac{L^2}{6t_L} \tag{2}$$

$$C_{app} = \frac{J_\infty L}{D_{eff}} \tag{3}$$

$$N_T = \frac{N_A \times C_{app}}{3}\left(\frac{D_1}{D_{eff}} - 1\right) \tag{4}$$

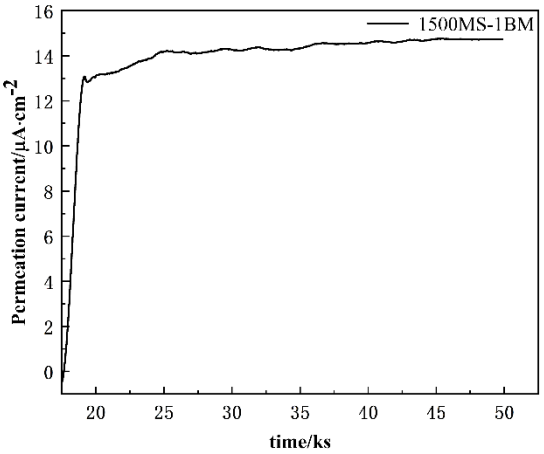

Figure 7. Hydrogen permeation curve of MS1500-1

Table 3. Hydrogen permeation parameters of MS1500-1

	L (mm)	I_∞ (μA)	t_L (s)	$J_\infty L$ (mol cm^{-1} s^{-1})	D_{eff} (cm^2 s^{-1})	C_{app} (mol cm^{-3})	N_T (cm^{-3})
MS-1BM	0.375	11.49	160	5.69×10-12	1.46×10-7	3.90×10-5	6.85×1021

4. CONCLUSION

This study provides a comprehensive experimental evaluation of the microstructural evolution, mechanical performance, and hydrogen permeation behavior of 1.5 GPa martensitic steel (MS1500-1) subjected to laser welding under various surface conditions. The key findings are summarized as follows:

Microstructural Characterization of Base Metal and Weld Zones: The MS1500-1 base metal consists of a uniformly distributed dual-phase microstructure of ferrite and martensite with a Body-Centered Cubic (BCC) structure. Laser welding induces a pronounced microstructural gradient. The fusion zone and coarse-grained heat-affected zone consist predominantly of coarse lath martensite due to rapid cooling from temperatures above Ac3. Conversely, the sub-critical heat-affected zone exhibits tempered martensite, leading to a significant softening effect with a hardness reduction of approximately 150–160 HV relative to the base metal.

Influence of Laser Welding Parameters and Surface Condition: For L-bend lap welding, a laser power of 3 kW, speed of 3.5 m/min, and defocus of -2 mm produced consistent joint penetration (≈3.4 mm) and width (≈1.0 mm). The presence of surface oil was found to influence the HAZ microstructure; specifically, the as-received oiled surface resulted in coarser martensite laths in the inter-critical HAZ and larger ferrite grains in the fine-grained HAZ compared to the oil-free condition. Under excessive oil conditions (3.0 g/m²), the hardened fine-grained zone exhibited a lower peak hardness (≈440 HV) and a wider softened zone width, suggesting that surface contamination alters the local cooling rates and carbon diffusion during welding.

Mechanical Properties and Hardness Distribution: Butt-welded joints achieved a tensile strength of up to 1131.7 MPa, reaching 73.1% of the base metal strength (1547.1 MPa). Microhardness mapping across the joints revealed a characteristic "M" shaped profile with distinct hardening and softening zones. The peak hardness (up to 482 HV) was consistently located in the fine-grained heat-affected zone due to grain refinement strengthening of the martensite, whereas the fusion zone hardness remained slightly lower (≈420–440 HV). The softened zone width was observed to increase with higher heat input and varied with surface oil contamination.

Hydrogen Permeation Behavior: Electrochemical hydrogen permeation tests on the MS1500-1 base metal revealed an effective hydrogen diffusion coefficient (D_{eff}) in the range of 1.46×10^{-7} to 2.13×10^{-7} cm²/s and a high apparent hydrogen concentration (C_{app}) of approximately 4.0×10^{-5} mol/cm³. The calculated hydrogen trap density (N_T) was on the order of $5–6 \times 10^{21}$ cm^{-3}. These values confirm a high density of reversible and irreversible hydrogen traps within the martensitic-ferritic matrix, which is a critical intrinsic factor governing the delayed cracking susceptibility of the welded joints.

In summary, the study demonstrates that while laser welding is effective for joining 1.5 GPa MS1500-1 steel, the resulting microstructural heterogeneity—specifically the softened HAZ and the high intrinsic hydrogen trap density—poses significant challenges for delayed cracking resistance. The findings underscore the necessity of strict surface cleanliness control and optimized heat input management to mitigate hydrogen-assisted degradation in automotive structural applications

REFERENCES

[1] Hadzipasic A, Malina J, Malina M. The influence of microstructure on hydrogen diffusion and embrittlement of fine-grained high strength dual-phase steels [J]. Kovove Materialy-Metallic Materials, Bratislava 38: Redakcia Kovove Materialy, 2021, 59(1): 69-78.

[2] Sun M, Wang X, Wang Z, et al. The critical impact of intercritical deformation on variant pairing of bainite/martensite in dual-phase steels [J]. Materials Science and Engineering: A, 2020, 771: 138668.

[3] Badkoobeh F, Nouri A, Hassannejad H, et al. Microstructure and mechanical properties of resistance spot welded dual-phase steels with various silicon contents [J]. Materials Science and Engineering a-Structural Materials Properties Microstructure and Processing, Lausanne: Elsevier Science Sa, 2020, 790: 139703.

[4] Sun J, Jiang T, Wang Y, et al. Ultrafine grained dual-phase martensite/ferrite steel strengthened and toughened by lamella structure [J]. Materials Science and Engineering a-Structural Materials Properties Microstructure and Processing, Lausanne: Elsevier Science Sa, 2018, 734: 311-317.

[5] Ashrafi H, Shamanian M, Emadi R, et al. A novel and simple technique for development of dual phase steels with excellent ductility [J]. Materials Science and Engineering: A, 2017, 680: 197-202.

[6] Sodjit S, Uthaisangsuk V. Microstructure based prediction of strain hardening behavior of dual phase steels [J]. Materials & Design, 2012, 41: 370-379.

[7] Le-yu Z, Ya-zheng L, Xue-wen H, et al. Effect of Alloying Element on Process Control of High Strength Hot-Rolled Dual Phase Steel [J]. Journal of Iron and Steel Research International, New York: Springer, 2011, 18: 792-795.